Received: 13 November 2020 | Accepted: 12 May 2021

DOI: 10.1111/nan.12736

Neuropathology and Applied Neurobiology WILEY

ORIGINAL ARTICLE

Balloon cells promote immune system activation in focal cortical dysplasia type 2b

Till S. Zimmer[1] | Diede W. M. Broekaart[1] | Mark Luinenburg[1] | Caroline Mijnsbergen[1] | Jasper J. Anink[1] | Nam Suk Sim[2] | Iliana Michailidou[3] | Floor E. Jansen[4] | Peter C. van Rijen[5] | Jeong Ho Lee[2,6] | Liesbeth François[7] | Jonathan van Eyll[7] | Stefanie Dedeurwaerdere[7,8] | Erwin A. van Vliet[1,9] | Angelika Mühlebner[1,10] | James D. Mills[1,11,12] | Eleonora Aronica[1,13]

[1]Department of (Neuro)Pathology, Amsterdam UMC, University of Amsterdam, Amsterdam Neuroscience, Amsterdam, The Netherlands

[2]Graduate School of Medical Science and Engineering, Korea Advanced Institute of Science and Technology (KAIST), Daejeon, Republic of Korea

[3]Department of Clinical Genetics, Leiden University Medical Centre, Leiden, The Netherlands

[4]Department of Paediatric Neurology, University Medical Center Utrecht, Utrecht, The Netherlands

[5]Department of Neurosurgery, Brain Center, Rudolf Magnus Institute for Neuroscience, University Medical Center Utrecht, Utrecht, The Netherlands

[6]SoVarGen, Inc, Daejeon, Republic of Korea

[7]Neurosciences Therapeutic Area, UCB Pharma, Braine-l'Alleud, Belgium

[8]Department of Translational Neuroscience, University of Antwerp, Wilrijk, Belgium

[9]Swammerdam Institute for Life Sciences, Center for Neuroscience, University of Amsterdam, Amsterdam, The Netherlands

[10]Department of Pathology, University Medical Center Utrecht, Utrecht, The Netherlands

[11]Department of Clinical and Experimental Epilepsy, UCL, London, UK

[12]Chalfont Centre for Epilepsy, Chalfont St Peter, UK

[13]Stichting Epilepsie Instellingen Nederland (SEIN), Heemstede, The Netherlands

Correspondence
Eleonora Aronica, Department of (Neuro) Pathology, Amsterdam UMC, University of Amsterdam, Meibergdreef 9, 1105 AZ Amsterdam, The Netherlands.
Email: e.aronica@amsterdamumc.nl

Funding information
Seventh Framework Programme, Grant/Award Number: 602391 and 602102; Horizon 2020 Framework Programme, Grant/Award Number: 952455; H2020 Marie Skłodowska-Curie Actions, Grant/Award Number: 722053; ZonMw, Grant/Award Number: 95105004; Epilepsiefonds, Grant/Award Number: 16-05, 20-11 and 20-02; UCB; Prinses Beatrix Spierfonds, Grant/Award Number: W.OR14

Abstract

Aims: Focal cortical dysplasia (FCD) type 2 is an epileptogenic malformation of the neocortex associated with somatic mutations in the mammalian target of rapamycin (mTOR) pathway. Histopathologically, FCD 2 is subdivided into FCD 2a and FCD 2b, the only discriminator being the presence of balloon cells (BCs) in FCD 2b. While pro-epileptogenic immune system activation and inflammatory responses are commonly detected in both subtypes, it is unknown what contextual role BCs play.

Methods: The present study employed RNA sequencing of surgically resected brain tissue from FCD 2a (n = 11) and FCD 2b (n = 20) patients compared to autopsy control (n = 9) focusing on three immune system processes: adaptive immunity, innate immunity and cytokine production. This analysis was followed by immunohistochemistry on a clinically well-characterised FCD 2 cohort.

Results: Differential expression analysis revealed stronger expression of components of innate immunity, adaptive immunity and cytokine production in FCD 2b than in FCD 2a, particularly complement activation and antigen presentation. Immunohistochemical

analysis confirmed these findings, with strong expression of leukocyte antigen I and II in FCD 2b as compared to FCD 2a. Moreover, T-lymphocyte tissue infiltration was elevated in FCD 2b. Expression of markers of immune system activation in FCD 2b was concentrated in subcortical white matter. Lastly, antigen presentation was strongly correlated with BC load in FCD 2b lesions.

Conclusion: We conclude that, next to mutation-driven mTOR activation and seizure activity, BCs are crucial drivers of inflammation in FCD 2b. Our findings indicate that therapies targeting inflammation may be beneficial in FCD 2b.

KEYWORDS
balloon cells, focal cortical dysplasia, immune system, inflammation

INTRODUCTION

Focal cortical dysplasia (FCD) represents a leading cause of drug-resistant focal epilepsy in children and young adults [1]. FCDs are characterised by focal, abnormal development of cortical layering and can be subdivided histopathologically into three categories: FCD 1 presents with abnormal radial or tangential organisation of the cortical layering, FCD 2 lacks any cortical organisation and contains additional cytological alterations, whereas FCD 3 is associated with other principal lesions such as hippocampal sclerosis, vascular malformations, tumours or lesions acquired during early life (e.g. trauma, ischaemia) [2,3].

Focal cortical dysplasia type 2 lesions are distinguished from other FCDs by dyslaminated cortical architecture, the presence of misplaced, cytomegalic dysmorphic neurons (DN) as well as reduced myelin content of the white matter (WM) and a blurring between WM and grey matter (GM) boundary [2]. Furthermore, FCD 2 can be sub-classified into FCD 2a and FCD 2b based on the presence of balloon cells (BC) in 2b [2], an immature cellular entity closely resembling giant cells (GCs) in tuberous sclerosis complex (TSC) [4]. Other diagnostic criteria include the 'transmantle sign', localised subcortically to the lesion on magnetic resonance imaging in FCD 2b, indicating WM damage [5–8].

Over the last decade, deep DNA sequencing of resected brain tissue from FCD 2 patients identified germline and/or brain somatic genetic abnormalities linked to aberrant activation of mammalian target of rapamycin (mTOR) signalling as genetic basis for the pathogenesis of FCD 2 [9–15]. The mTOR-signalling cascade is crucially involved in the integration of environmental stimuli to regulate proliferation, metabolism and cell growth [16]. Thus, the currently accepted hypothesis proposes that mTOR-pathway hyperactivation during brain development produces cellular hypertrophy and aberrant migration in FCD 2.

Apart from the principal cyto-architectural abnormalities, activation of the immune system and production of pro-inflammatory mediators are typical features of lesions in FCD 2 [17]. More specifically, activation of the innate immune system, recruitment of peripheral immune cells and release of pro-inflammatory cytokines, such as interleukin (IL)-1β, can be detected [18–24]. Although these reactive changes are likely secondary to the principal lesion, mounting evidence suggests that inflammation plays a crucial role in seizure generation, epileptogenesis and chronic epilepsy [17,25,26]. Therefore, a better understanding of the specific inflammatory pathways activated in FCD 2 could aid in a better understanding of aberrant brain development and the resulting neurological symptoms. Moreover, the role of BCs as histopathological discriminator between FCD 2b and FCD 2a in relation to neuroinflammation remains enigmatic.

We performed RNA sequencing (RNA-Seq) on surgically resected tissue from a cohort of 31 FCD 2 patients to assess possible 2a/2b subtype-specific regulation of the immune system. This analysis was followed by immunohistochemical evaluation of innate and adaptive immune system activation in a subset of 16 patients with identified genetic alterations in mTOR-pathway components. To this end, we aimed to understand whether the histopathological differences between FCD 2a and FCD 2b also translate to immune system regulation.

MATERIALS AND METHODS

Subjects

Brain tissues included in this study were obtained from the archives of the Departments of Neuropathology of the Amsterdam UMC (Amsterdam, The Netherlands) and the UMC Utrecht (Utrecht, The Netherlands). Cortical brain samples were obtained from patients undergoing surgery for intractable epilepsy and diagnosed with FCD 2 (n = 11 FCD 2a, n = 20 FCD 2b). All cases were reviewed independently by two neuropathologists. Patients who underwent implantation of strip and/or grid electrodes for chronic subdural invasive monitoring before resection and patients who underwent previous resective epilepsy surgery were excluded from this study. The diagnosis of FCD was confirmed according to the international consensus classification system proposed for grading FCD [2]. None of the FCD patients fulfilled the diagnostic criteria for TSC. For RNA sequencing, a control group (n = 9) of age and brain area-matched

autopsy tissue was included. Patients donating autopsy control tissue did not have a history of seizures or other neurological diseases. All autopsies were performed within 24 h after death. For immunohistochemical analysis, 16 FCD 2 cases with identified mutations (Table S1 and S2) and histopathological subclassification into 2a and 2b were selected. The samples used for immunohistochemistry underwent deep sequencing using DNA extracted from snap-frozen surgical brain tissue targeting 13 genes (Table S3; FCD panel SoVarGen, Korea). Analysis for replicated data was performed in accordance with a previous study [15]. For the validation of our immunohistological findings, we employed an additional, independent group of histopathologically defined FCD 2 cases (n = 15) from our archives. Clinical details of patient cohorts used in this study are summarised in Table S2. FCD 2a and FCD 2b cases differed in age and epilepsy duration, but not seizure frequency (Figure S1M–O). Tissue was obtained with informed consent for the use in research and access to medical records in accordance with the Declaration of Helsinki and the Amsterdam UMC Research Code provided by the Medical Ethics Committee.

Immunohistochemistry

Immunohistochemistry on paraffin-embedded tissue from resected FCD 2a, 2b and autopsy control tissue as well as quantification of staining was performed as described in Supplementary Methods. For FCD 2a and 2b, a panel of markers (haematoxylin and eosin [H&E], phosphorylated S6 [pS6 as marker of mTOR-pathway activation], neurofilament; Figure S1) was used to define the region of interest. Immunohistochemistry employed 7 FCD 2a (3 *DEPDC5*/3 *AKT3*/1 *MTOR*) and 9 FCD 2b (8 *MTOR*/ 1 *TSC1*) cases (Table S2). The sub-selection of these 16 cases was based on the completeness of clinical information as well as on the availability of frozen and paraffin-embedded tissue.

Bioinformatics analysis of RNA-Seq data

Representative frozen tissue to be used for RNA sequencing was identified using H&E and pS6 immunohistochemistry on frozen sections. RNA sequencing employed 11 FCD 2a (10 cases with identified mutation: 4 *DEPDC5*/3 *AKT3*/2 *MTOR*/1 *NPLR3*) and 21 FCD 2b (12 cases with identified mutations: 11 *MTOR*/ 1 *TSC1*) cases, including the cohort used for immunohistochemistry (Table S2). RNA isolation, quality control and sequencing were performed as described in Supplementary Methods.

Differential expression analysis was carried out using the R package limma. For each differential expression analysis, genes from the reactome pathways [27] innate immune system (R-HSA-168249), adaptive immune system (R-HSA-1280218) and cytokine signalling in immune system (R-HSA-1280215) were extracted. Subsequently, a linear model was fit for each gene and moderated t-statistic was calculated after applying an empirical Bayes smoothing to the standard errors. Those genes with a Benjamini–Hochberg adjusted p value < 0.05 were considered differentially expressed.

To assess the similarities between the expression profiles of each set of genes in each pathway of interest, the Euclidean distance was calculated. These results were then visualised as heatmaps in R. To assess which specific sub-categories of genes were altered in each of these pathways, a gene ontology (GO) enrichment analysis using the differentially expressed genes in each pathway from each comparison as an input and the specific pathway as the gene background was performed using the Database for Annotation, Visualization and Integrated Discovery (DAVID) v6.8 [28]. Gene ontology terms with Benjamini–Hochberg adjusted p value < 0.05 were considered enriched. The enriched GO terms were visualised using the enrichmentMap plugin in cytoscape [29].

Statistical analysis

Statistical analysis was performed with GraphPad Prism software version 5.01 (Graphpad software Inc.) using the non-parametric Mann–Whitney U-test. $p < 0.05$ was assumed to indicate a significant difference. Data are presented as scatter plots with median. Correlation analysis was performed using Spearman's rank correlation. For RNA-Seq data, a Mann–Whitney U-test followed by a Benjamini–Hochberg correction for multiple comparison test was carried out. An adjusted $p < 0.05$ was assumed to indicate statistical significance.

RESULTS

Although it is tempting to speculate about the role of somatic mutations in the pathogenesis of FCD 2a and 2b, current studies (including the one presented here) trying to link genotype to histopathology of FCD 2a/2b are limited by the low number of cases with detected mutations. Nonetheless, we aimed to show expression of the individual genotypes in this study (number of patients with mTOR-pathway mutations: *MTOR*: 8 FCD 2b, 1 FCD 2a; *DEPDC5*: 3 FCD 2a; *AKT3*: 3 FCD 2a; *TSC1*: 1 FCD 2b) to be potentially comparable to genetically characterised cohorts of future studies. Since we found strong differences between histopathological subtypes rather than genotype, we grouped histopathologically defined FCD 2a and FCD 2b cases and compared them to each other. Since we knew from preliminary data that FCD 2a and FCD 2b differ at the immunohistochemical level, we aimed to compare the differentially expressed genes versus control from each FCD 2 subtype and compared these datasets to each other to increase overall sensitivity. Detailed description of RNA-Seq data and additional immune cell markers for each pathway is found in Supporting Information (Figures S2 and S3; Table S5).

Adaptive immune system activation, T-lymphocyte recruitment and antigen presentation are higher in FCD 2b

To investigate the activation of the adaptive immune system in FCD 2a and FCD 2b lesions, we investigated the differential expression of a set of genes associated with adaptive immunity retrieved from the Reactome pathway database. Differential expression analysis detected 88 upregulated and 12 downregulated genes in FCD 2a cases and 173 upregulated and 68 downregulated genes in FCD 2b lesions (Figure 1A). Of the upregulated genes, 83 were common between FCD 2a and FCD 2b while 90 were specific for FCD 2b and 5 for FCD 2a (Figure 1B). From the set of downregulated genes, 10 genes were common between FCD 2a and FCD 2b while 58 genes were specifically downregulated in FCD 2b and 2 in FCD 2a (Figure 1B).

Gene ontology analysis of upregulated genes revealed common terms including immune response, plasma membrane and integral component of membrane. In addition, FCD 2b specifically revealed enrichment of GO terms involved in antigen processing and presentation on HLA-II protein complex, as well as interferon-gamma-mediated signalling (Figure 1C).

Immunohistochemical evaluation of FCD 2 tissue for CD3 revealed intra-parenchymal $CD3^+$ cells in FCD 2b cases (Figure 1D,G), but not in FCD 2a where they were found almost exclusively intravascular or perivascular (Figure 1E,F). Quantification of relative CD3 count showed a higher total CD3 cell count in lesions of FCD 2b cases (Figure 1H,I). We found overall very few $CD4^+$ cells in FCD 2b and almost none in FCD 2a cases (Figure S1V–Y). The fraction of $CD8^+$ T lymphocytes we detected was higher than $CD4^+$ cells (Figure 1J–M). Again, FCD 2b cases displayed a higher relative number of $CD8^+$ cells than FCD 2a (Figure 1N,O). There was no difference in the localisation of $CD4^+$/$CD8^+$ cells compared to $CD3^+$ (intravascular/perivascular in FCD 2a vs. intra-parenchymal in FCD 2b). HLA-I expression could be found in vessels and DNs in FCD 2a and FCD 2b (Figure 1P–S); however, fewer DNs expressed HLA-I in FCD 2a than in FCD 2b (Figure 1Q, arrows). BCs in FCD 2b did not show prominent HLA-I expression while small, glial cells displayed very high expression specifically in FCD 2b (Figure 1P,S). Moreover, the BC-rich subcortical WM displayed very strong expression (Figure 1S). Quantification of HLA-I revealed higher expression in FCD 2b, especially one FCD 2b case with *TSC1* mutation (Figure 1S,T). Expression of HLA-II was primarily detected in cells with microglial/macrophage morphology as well as some BCs in FCD 2b (Figure 1V,Y). Besides one FCD 2a case with *DEPDC5* mutation, we could not detect HLA-II expression in FCD 2a cases (Figure 1W,X,Z). Quantification of HLA-II revealed higher expression in FCD 2b cases (Figure 1AA). The expression of the investigated markers did not correlate with seizure frequency or age (Table S4).

Total number of $CD68^+$-cells and expression of translocator protein are enhanced in FCD 2b versus FCD 2a

Analysis of the innate immunity gene set revealed 161 upregulated and 28 upregulated genes for FCD 2a and 288 upregulated and 80 downregulated genes for FCD 2b (Figure 2A). Of the upregulated genes, 156 were common between FCD 2a and FCD 2b while 132 were specific for FCD 2b and 5 for FCD 2a (Figure 2B). From the set of downregulated genes, 20 genes were common between FCD 2a and FCD 2b while 60 genes were specifically downregulated in FCD 2b and 8 in FCD 2a (Figure 2B).

Gene ontology analysis of upregulated genes revealed inflammatory response as common differentially regulated mechanism. In addition, FCD 2a gene expression enriched for plasma membrane components (Figure 2C).

Evaluation of Iba1 expression as indicator of total microglial density did not reveal differences between FCD 2a and FCD 2b (Figure 2H,I); however, we frequently detected a more activated morphological phenotype in FCD 2b (Figure 2D,G) versus FCD

FIGURE 1 Adaptive immune activation, T-lymphocyte infiltration and antigen presentation are higher in FCD 2b than in FCD 2a lesions. Volcano plots of differentially expressed genes in the adaptive immunity gene set reveal 88 upregulated and 12 downregulated genes in FCD 2a and 173 upregulated and 68 downregulated genes in FCD 2b lesions, respectively (A). Venn diagrams of the upregulated and downregulated genes reveal a higher proportion of FCD 2b-specific genes compared to FCD 2a (B). Gene ontology analysis revealed changes of plasma membrane components and immune response overall in both FCD 2a and FCD 2b. However, FCD 2b exclusively revealed activation of pathways involved in antigen processing and presentation as well as interferon-gamma-mediated signalling (C). Representative micrographs show lesions diagnosed as FCD 2b with *MTOR* mutation (D,J,P,V), FCD 2a with *DEPDC5* mutation (E,K,Q,W), FCD 2a with *AKT3* mutation (F,L,R,X) and FCD 2b with *TSC1* mutation (G,M,S,Y). Immunohistochemical evaluation of $CD3^+$ T lymphocytes revealed an overall higher number of T lymphocytes in FCD 2b lesions and these cells were often found associated with dysmorphic cells in the tissue (D,G,H,I). In contrast, FCD 2a lesions revealed T lymphocytes predominantly in vessels and only occasionally infiltrating the brain parenchyma (E,F, arrows). Of the total T-lymphocyte population, $CD8^+$ cells could be found to infiltrate FCD 2b tissue, with overall more $CD8^+$ cells (J,M,N,O) compared to FCD 2a (K,L,N,O). HLA-I expression could be found in vessels and DNs in FCD 2a lesions (Q,R,T,U) while overall stronger expression was detected in DNs, the neuropil and glia, but not BCs in FCD 2b lesions (P,S,T,U). HLA-II expression in FCD 2a lesions was detected only in vessels (W,X,Z,AA) while FCD 2b lesions revealed much stronger expression in BCs and cells with microglial morphology (V,Y,Z,AA). Sections were counterstained with haematoxylin. Scale bars: 50 μm in D (representative for D–G,J–M,P–S,V–Y), arrows D–G, J–M = T lymphocytes; arrows P–S, V–Y = DN. Mann–Whitney *U*-test. Data are displayed as scatter plot (green = FCD 2b; blue = FCD 2a) with median; $^*p < 0.05$, $^{**}p < 0.01$. A–C $n = 9$ autopsy control, $n = 11$ FCD 2a, $n = 20$ FCD 2b cases. D–AA $n = 7$ FCD 2a and $n = 9$ FCD 2b cases. BC, balloon cell; DN, dysmorphic neuron; FCD, focal cortical dysplasia; TSC, tuberous sclerosis complex

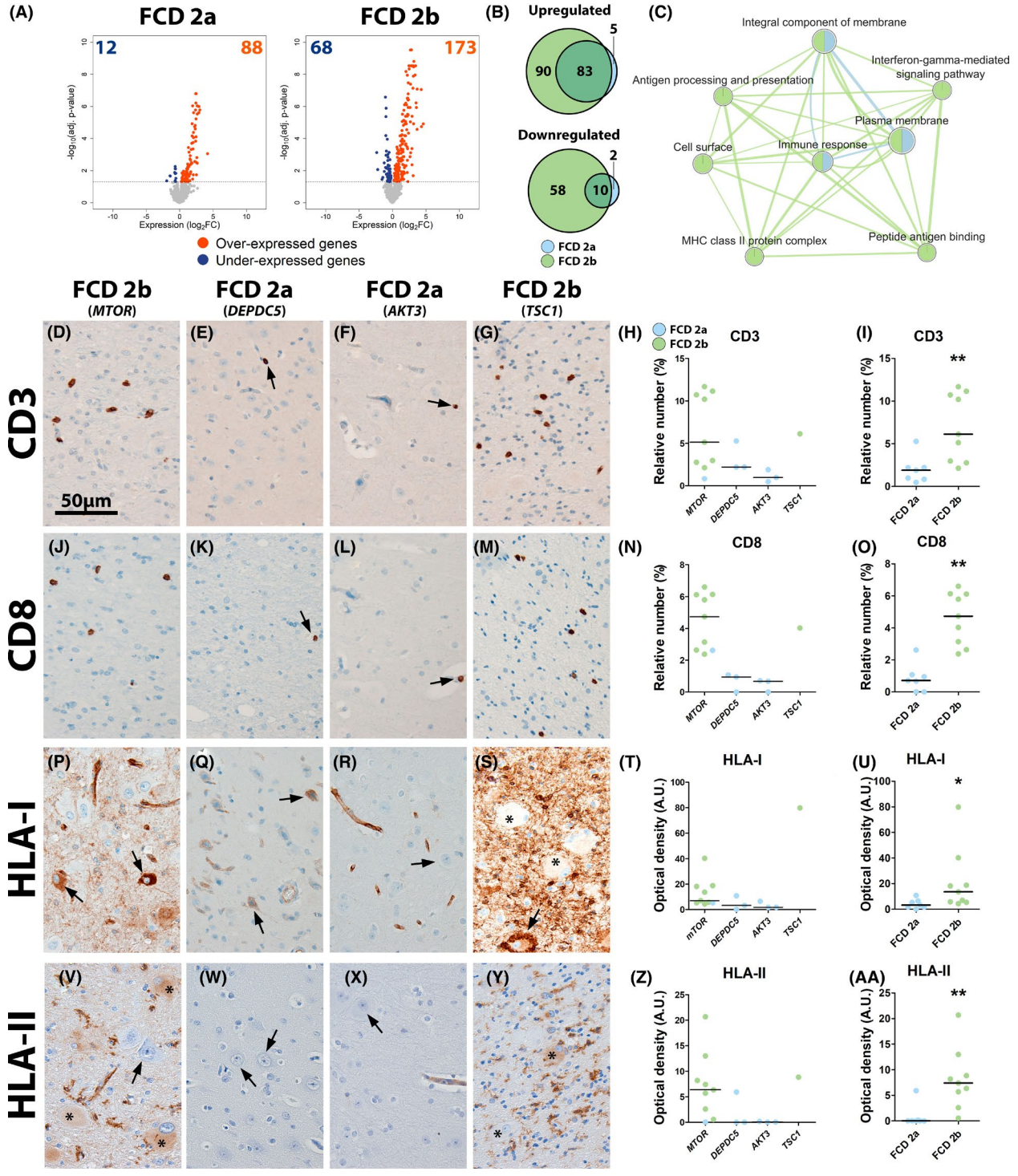

2a (Figure 2E,F). Next, we investigated CD68 as indicator of total monocytes and macrophages. CD68 reactivity was high, especially around malformed cells in FCD 2a and FCD 2b (Figure 2J–M). Quantification revealed an overall higher CD68 expression in FCD 2b versus FCD 2a (Figure 2N,O). TSPO expression could be detected in microglia, BCs and some DNs (Figure 2P–S). Overall, FCD 2b cases displayed very strong expression in BCs and the neuropil as compared to FCD 2a (Figure 2P,S). Quantification of TSPO density confirmed these findings (Figure 2T,U). The expression of the investigated markers did not correlate with seizure frequency or age (Table S4).

Expression of cytokine-related processes and chemoattractants is enhanced in FCD 2b versus FCD 2a

The cytokine gene set revealed 87 upregulated and 19 downregulated genes for FCD 2a and 197 upregulated and 63 downregulated genes

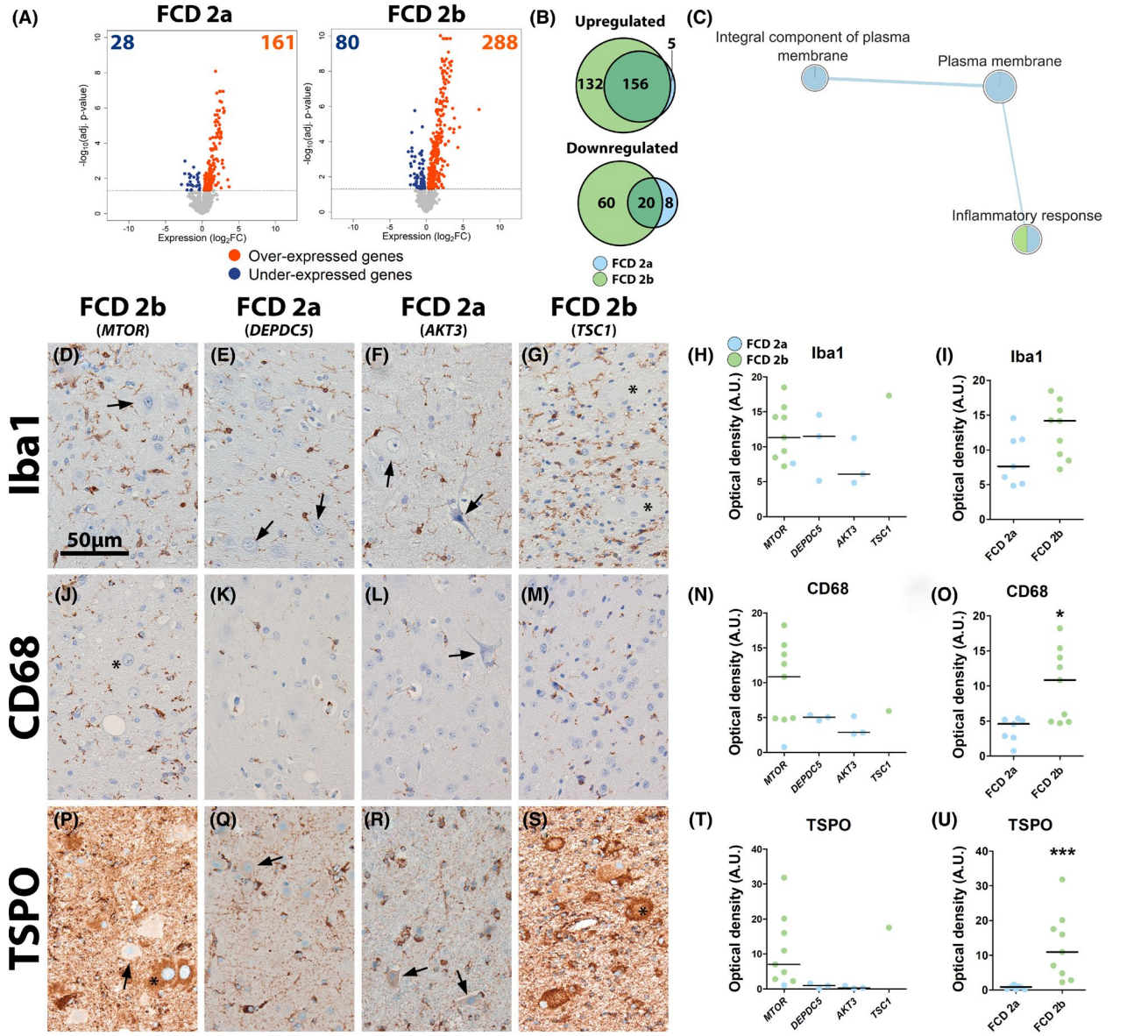

FIGURE 2 Microglia and peripheral macrophage activation are higher in FCD 2b than in FCD 2a lesions. Volcano plots of differentially expressed genes in the innate immunity gene set reveal 161 upregulated and 28 downregulated genes in FCD 2a and 288 upregulated and 80 downregulated genes in FCD 2b lesions, respectively (A). Venn diagrams of the upregulated and downregulated genes reveal a higher proportion of FCD 2b-specific genes compared to FCD 2a (B). Gene ontology analysis revealed changes of plasma membrane components in FCD 2a and inflammatory response overall in both FCD 2a and FCD 2b. (C). Representative micrographs show lesions diagnosed as FCD 2b with *MTOR* mutation (D,J,P), FCD 2a with *DEPDC5* mutation (E,K,Q), FCD 2a with *AKT3* mutation (F,L,R) and FCD 2b with *TSC1* mutation (G,M,S). Immunohistochemical evaluation of Iba1^{+} microglia revealed no difference in microglia number between FCD 2a versus FCD 2b lesions, though microglia presented with an overall activated, less ramified morphology (D–I). On the contrary, CD68 showed higher expression in FCD 2b than in FCD 2a (J–O). TSPO expression could be found in microglia and the neuropil (P–S), as well as BCs in FCD 2b (P,S). Overall, higher TSPO expression could be detected in FCD 2b versus FCD 2a lesions (P–U). Sections were counterstained with haematoxylin. Scale bars: 50 µm in D (representative for D–G, J–M, P–S), arrows = DNs; asterisk = BCs. Mann–Whitney *U*-test. Data are displayed as scatter plot (green = FCD 2b; blue = FCD 2a) with median; $^{*}p < 0.05$, $^{***}p < 0.001$. A–C $n = 9$ autopsy control, $n = 11$ FCD 2a, $n = 20$ FCD 2b cases. D–U $n = 7$ FCD 2a and $n = 9$ FCD 2b cases. BC, balloon cell; DN, dysmorphic neuron; FCD, focal cortical dysplasia; TSC, tuberous sclerosis complex

for FCD 2b (Figure 3A). Of the upregulated genes, 87 were common between FCD 2a and FCD 2b while 110 were specific for FCD 2b and none for FCD 2a (Figure 3B). Of the set of downregulated genes, 13 genes were common between FCD 2a and FCD 2b while 50 genes were specifically downregulated in FCD 2b and 6 in FCD 2a (Figure 3B).

Gene ontology term analysis of upregulated genes yielded FCD 2b-specific enrichment for vesicular transport, cell surface as well as cytokine-mediated signalling pathway (Figure 3C).

Immunohistochemical investigation of IL-17 in FCD 2a and FCD 2b tissue revealed strong expression in DNs and scattered cells

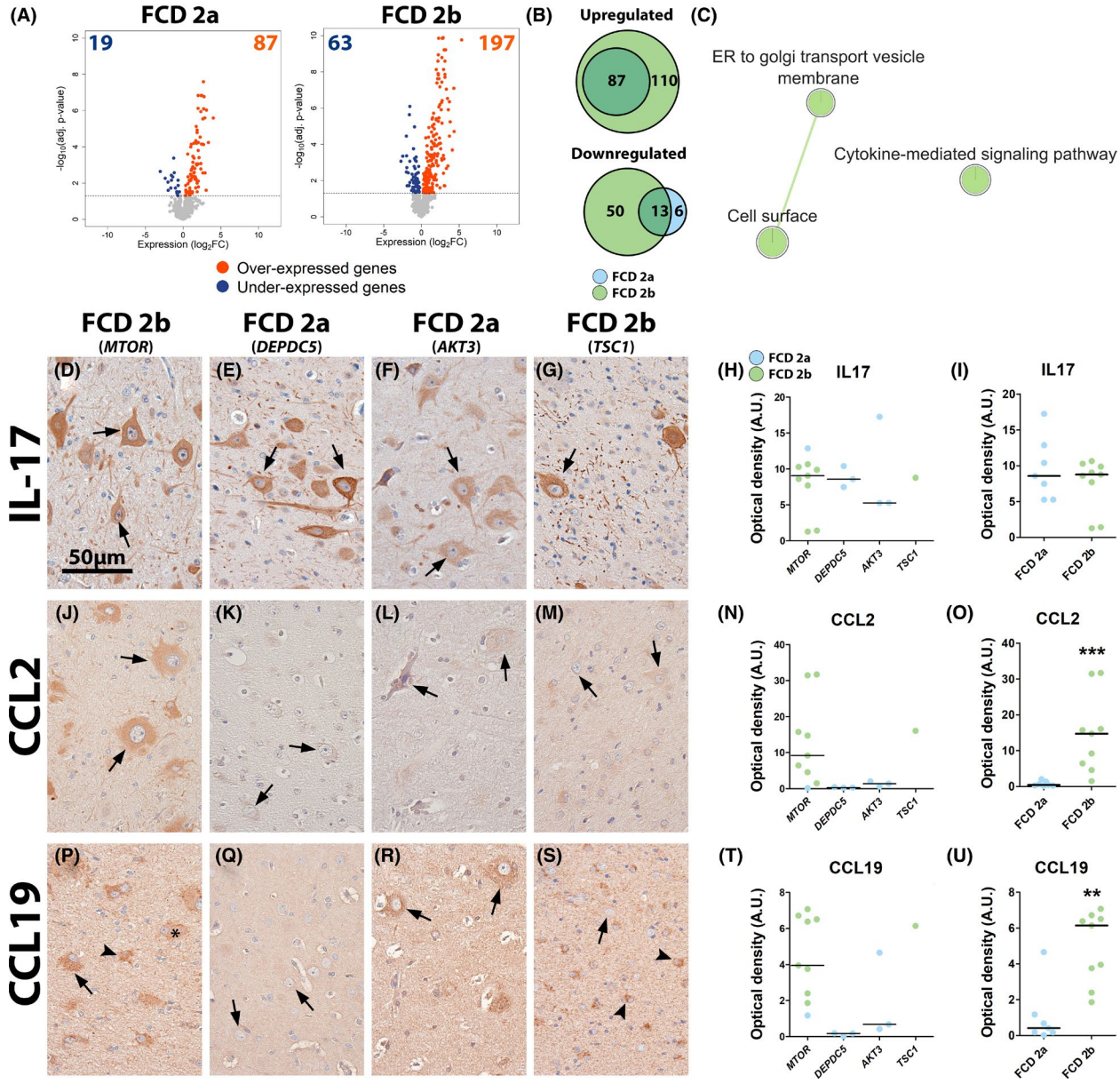

FIGURE 3 Cytokine expression, in particular of chemo-attractants is elevated in FCD 2b lesions versus FCD 2a. Volcano plots of differentially expressed genes in the cytokine gene set reveal 87 upregulated and 19 downregulated genes in FCD 2a and 197 upregulated and 63 downregulated genes in FCD 2b lesions, respectively (A). Venn diagrams of the upregulated genes reveal that the whole set of upregulated genes of FCD 2a are contained in FCD 2b. Downregulated genes reveal a higher proportion of FCD 2b-specific upregulated genes. (B). Gene ontology analysis of the cytokine gene set reveals changes solely in FCD 2b and these processes are connected to cytokine signalling but also membrane trafficking (C). Representative micrographs show lesions diagnosed as FCD 2b with *MTOR* mutation (D,J,P), FCD 2a with *DEPDC5* mutation (E,K,Q), FCD 2a with *AKT3* mutation (F,L,R) and FCD 2b with *TSC1* mutation (G,M,S). Immunohistochemical evaluation of IL-17 showed strong expression in DNs and dysmorphic neurites. FCD 2a and FCD 2b IL-17 expression did not differ (D–I). Strong expression of CCL2 was detected in BCs and weakly in DNs in FCD 2b while staining in FCD 2a lesions was low to undetectable (J–M). Overall, FCD 2b lesions presented with stronger CCL2 expression (N,O). CCL19 expression was detected in BCs, DNs and (dysplastic) glia (P–S). Quantification revealed a higher expression in FCD 2b lesions compared to FCD 2a (T,U). Sections were counterstained with haematoxylin. Scale bars: 50 µm in D (representative for D–G, J–M, P–S, V–Y), arrows = DNs; arrowheads = (dysplastic) glia; asterisk = BCs. Mann–Whitney *U*-test. Data are displayed as scatter plot (green = FCD 2b; blue = FCD 2a) with median; $^{**}p < 0.01$, $^{***}p < 0.001$. A–C $n = 9$ autopsy control, $n = 11$ FCD 2a, $n = 20$ FCD 2b cases. D–U $n = 7$ FCD 2a and $n = 9$ FCD 2b cases. BC, balloon cell; DN, dysmorphic neuron; FCD, focal cortical dysplasia; TSC, tuberous sclerosis complex

with leukocyte morphology (Figure 3D–G). Quantification of IL-17 expression did not reveal a difference between FCD 2a and FCD 2b (Figure 3H,I). On the contrary, the chemokines CCL2 and CCL19 displayed strong expression in BCs as well as normal-appearing and dysplastic astrocytes in FCD 2b and only low expression in DNs in FCD 2a and FCD 2b (Figure 3J–M,P–S). Additionally, normal

appearing astrocytes in the WM showed expression of CCL2 and CCL19 (Figure 3M,S, arrowheads). Quantification of both chemokines revealed stronger expression in FCD 2b versus FCD 2a (Figure 3N,O,T,U). CCL19 was negatively correlated with seizure frequency (ρ = −0.5177, p = 0.04) (Table S4).

DN in FCD 2a and FCD 2b express pro-inflammatory mediators and markers of oxidative stress

Although FCD 2b appeared to display stronger activation and recruitment of the immune system, inflammatory processes are reported for both FCD 2 subtypes. Therefore, we aimed to compare the expression of inducible pro-inflammatory markers, secondary to immune system activation, previously shown to be expressed strongly in malformed cells between FCD 2a and FCD 2b. We detected strong COX-2 expression in DNs in FCD 2a and FCD 2b (Figure 4A–D). Of note, all lesions from patients with *DEPDC5* mutations had very strong COX-2 expression, likely due to the high density of DNs (Figure 4E). Nevertheless, FCD2a and FCD2b did not differ (Figure 4F). Next, we investigated the expression of iNOS, a marker shown to be highly expressed in BCs and neurons. We found low expression of iNOS in normal appearing neurons and stronger expression in normal and dysplastic astrocytes, as well as DNs (Figure 4G–J). Moreover, sparsely distributed BCs displayed very strong expression of iNOS, leading to overall stronger expression in FCD 2b compared to FCD 2a (Figure 4K,L). Finally, we investigated expression of the inducible anti-oxidant gene HO-1, which was expressed in DNs and BCs (Figure 4M–P). Quantification did not signify a difference between FCD 2a and FCD 2b, but two out of the three FCD 2a lesions with *AKT3* mutation displayed very strong HO-1 expression (Figure 4Q,R). HO-1 expression was negatively correlated with seizure frequency (ρ = −0.5944, p = 0.0152) while iNOS (ρ = 0.6041, p = 0.0132) and HO-1 (ρ = 0.5598, p = 0.0241) were positively correlated with age (Table S4).

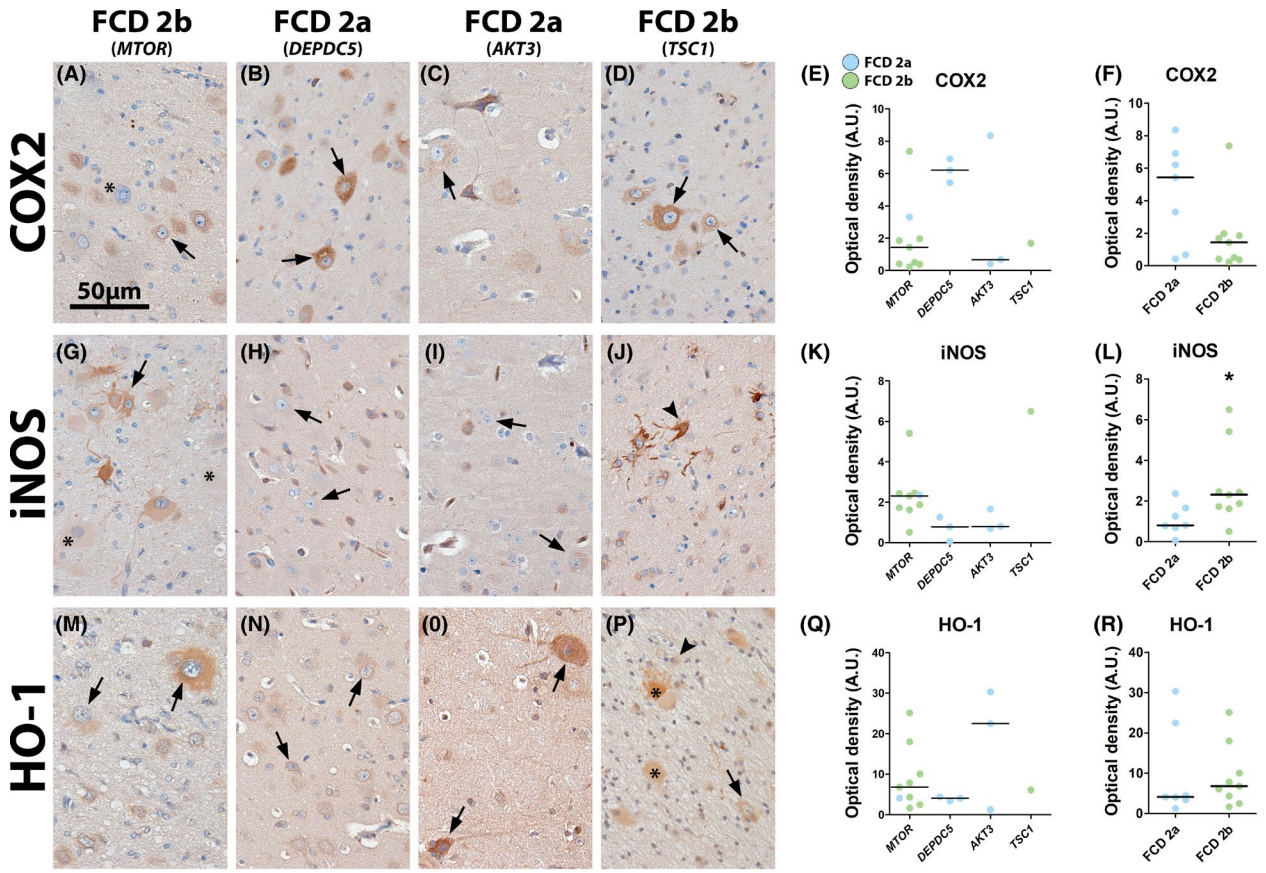

FIGURE 4 Expression of inducible stress genes is prominent in DN in FCD 2a and FCD 2b lesions. Representative micrographs show lesions diagnosed as FCD 2b with *MTOR* mutation (A,G,M), FCD 2a with *DEPDC5* mutation (B,H,N), FCD 2a with *AKT3* mutation (C,I,O) and FCD 2b with *TSC1* mutation (D,J,P). Strong COX-2 expression was found mainly in DNs and some glia (A-D). Quantification of COX-2 expression revealed high expression in *DEPDC5* FCD 2a lesions, but no difference between FCD 2a versus FCD 2b lesions (E,F). Expression of iNOS could be found strongest in BCs, followed by glia and DNs (G–J). Quantification of total expression showed higher expression in FCD 2b lesions, attributed mostly to the very strong expression in some BCs (K,L). Expression of HO-1 could be found in DNs and some BCs as well as glia (M–P); however, FCD 2a and FCD 2b expression did not differ. Sections were counterstained with haematoxylin. Scale bars: 50 µm in A (representative for A–D,G–J,M–P), arrows = DNs; arrowheads = (dysplastic) glia; asterisk = BCs. Mann–Whitney *U*-test. Data are displayed as scatter plot (green = FCD 2b; blue = FCD 2a) with median; *p < 0.05. n = 7 FCD 2a and n = 9 FCD 2b cases. BC, balloon cell; DN, dysmorphic neuron; FCD, focal cortical dysplasia; TSC, tuberous sclerosis complex

Complement expression is common in FCD 2a and FCD 2b lesions and precipitates around BCs

Since prior studies and our RNA-Seq dataset reported overexpression of complement components in FCD 2a and FCD 2b, we aimed at characterising early components of the complement system, namely C1q and the final product of C3 cleavage, C3d. C1q expression was strongly expressed in GM lesions around DNs in FCD 2a and FCD 2b and around BCs in FCD 2b (Figure 5A–C,F). Here, BC-rich regions in FCD 2b lesions displayed stronger reactivity than the tissue surrounding these areas (Figure 5E, arrows). In contrast, C1q expression was detected in cell processes in WM lesions (Figure 5D). Moreover, C1q expression could be detected occasionally around vessels (Figure 5G). C3d expression was detected around DNs, BCs, dysplastic astrocytes in the GM and astrocytes in the WM (Figure 5H–K,M,N). Similar to C1q, zones rich in malformed cells displayed stronger C3d reactivity than the surrounding tissue, though this difference was not as pronounced as for C1q (Figure 5L, arrows). Importantly, we did not detect any C9/C9neo reactivity, the marker for the membrane attack complex, the terminal product of complement activation, in either FCD 2a or FCD 2b (Figure S2E,F). Extraction of complement genes from the RNA-Seq dataset revealed an overall stronger upregulation of complement factors in FCD 2b versus FCD 2a, in particular early complement factors C1–C4; however, no individual factor was statistically different between the two subtypes (Figure 5O).

T-lymphocyte recruitment and antigen presentation are concentrated in BC-rich FCD 2b lesions and correlate with WM damage

Since $CD3^+$ cells and HLA-II expression displayed clear differences between FCD 2a and FCD 2b, another FCD cohort from our

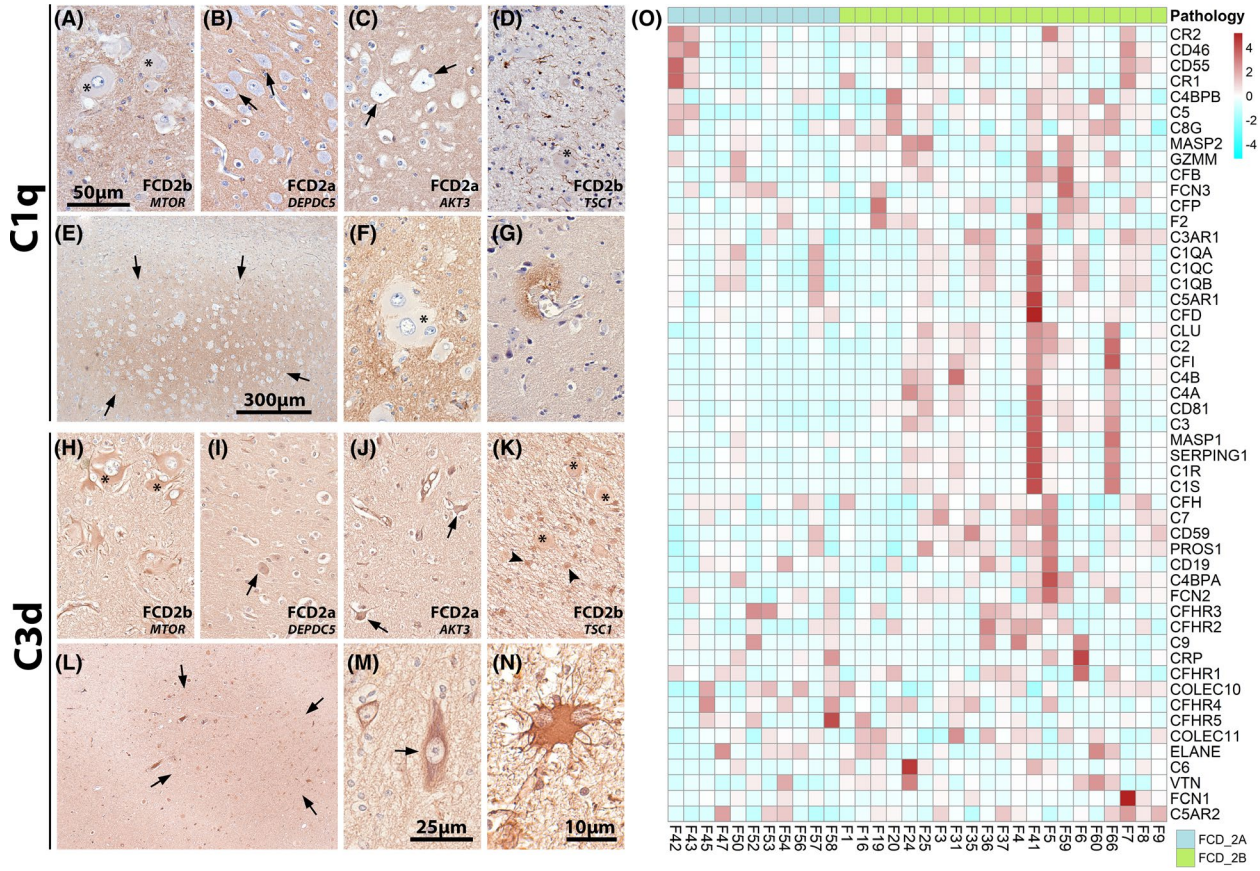

FIGURE 5 Complement components are strongly expressed in FCD 2 and concentrate around BC-rich lesions in FCD 2b. Representative micrographs show lesions diagnosed as FCD 2b with *MTOR* mutation (A,H), FCD 2a with *DEPDC5* mutation (B,I), FCD 2a with *AKT3* mutation (C,J) and FCD 2b with *TSC1* mutation (D,K). Expression of C1q could be detected solely in the neuropil (A–C) and occasionally in cellular processes in areas resembling white matter (D). High C1q expression could be found around BCs in FCD 2b (E,F) and occasionally perivascular (G). C3d expression was detected in DNs (M) and BCs likewise (H–J) and occasionally also in dysplastic glia (K,N). Complement factor gene expression was activated in both FCD 2a and FCD 2b, with generally higher expression in FCD 2b, though no single complement factor was different between FCD 2a versus FCD 2b (O). Sections were counterstained with haematoxylin. Scale bars: 50 µm in A (representative for B–D,F,G,H–K), 300 µm in E (representative for L), 25 µm in M, 10 µm in N, arrows = DNs; arrowheads = dysplastic glia; asterisk = BCs. A–N n = 7 FCD 2a and n = 9 FCD 2b cases, O n = 11 FCD 2a and n = 20 FCD 2b cases. BC, balloon cell; DN, dysmorphic neuron; FCD, focal cortical dysplasia; TSC, tuberous sclerosis complex

archives was employed for validation of these markers. The presence of intraparenchymal $CD3^+$ cells in FCD 2b could be validated and, similar to the main cohort, tissue infiltration of T lymphocytes was very sparse in FCD 2a (Figure 6A). Since we detected markedly more $CD3^+$ cells in BC-rich WM, we compared $CD3^+$ counts between GM and WM in the same lesion, but could not detect a difference (Figure 6B,D). Of note, the total number of $CD3^+$ cells was much higher in some regions of the WM (Figure 6C); however, due to the high cellularity of the WM, the relative $CD3^+$ cell count was not higher. The difference in antigen presentation as indicated by HLA-II expression between FCD 2a and FCD 2b was conserved in our validation cohort (Figure 6E). Also, here we detected visual differences between GM and WM (Figure 6F,G), and quantification confirmed higher expression in subcortical WM rich in BCs (Figure 6H). Evaluation of HLA genes from the RNA-Seq dataset revealed overall stronger expression in FCD 2b compared to FCD 2a (Figure 6I, asterisk indicates difference). On the individual gene level, primarily HLA-D family genes were upregulated in FCD 2b compared to FCD 2a. The number of $CD3^+$ cells was positively correlated with HLA-II expression (Figure 6J; $\rho = 0.7317$, $p < 0.0001$). As for HLA-II, a difference in expression between GM and subcortical WM could also be detected for HLA-I (Figure 6K) as well as CCL2 (Figure 6L). Co-labelling revealed expression of HLA-I with Olig2 (Figure $6K_1$) and NeuN expressing normal appearing neurons (Figure $6K_2$) and DNs. Of note, DNs expressed more HLA-I in areas with high HLA-I expression in the neuropil and *vice versa* (not shown). Moreover, we found a strong correlation of HLA-II expression and BC density (Figure 6M; $\rho = 0.556$, $p = 0.0006$). Finally, we also assessed the subcortical WM and found negative correlations of oligodendrocyte number ($\rho = -0.5523$, $p < 0.0007$) and myelin ($\rho = -0.5386$, $p < 0.0031$) with HLA-II (Figure 6N,O). Here, areas of high HLA-II reactivity displayed low oligodendrocyte count and low MBP density (Figure 6N,O, top panel) and *vice versa* (Figure 6N,O, bottom panel).

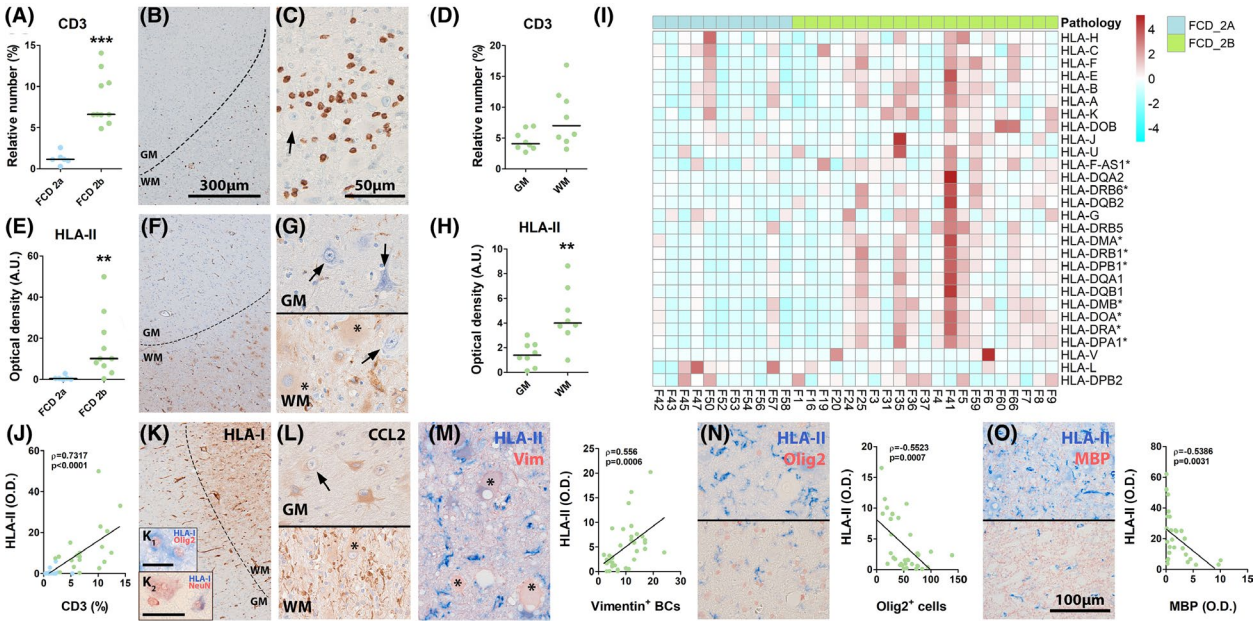

FIGURE 6 Antigen presentation and lymphocyte recruitment are more pronounced in subcortical white matter (WM) with high numbers of BCs in FCD 2b. Higher number of $CD3^+$ cells infiltrating the brain parenchyma in FCD 2b versus FCD 2a could be confirmed employing an independent cohort for immunohistochemical evaluation (A). Detailed examination of FCD 2b lesions detected $CD3^+$ cells mostly in subcortical areas that resembled improperly developed WM (B), with occasional dense clustering (C). No difference in relative $CD3^+$ cell count could be detected in FCD 2b lesions when comparing grey to WM (D). As for CD3, stronger HLA-II expression in FCD 2b lesions was confirmed in an independent immunohistochemistry validation cohort (E). Moreover, stronger expression of HLA-II could be detected in subcortical WM of FCD 2b lesions compared to grey matter (F–H). Heatmap of HLA genes revealed a stronger upregulation of all HLA genes in FCD 2b cases as compared to FCD 2a, especially of the HLA-D family (I). For the total cohort, $CD3^+$ cells and HLA-II expression were strongly correlated (J). As for HLA-II, we also detected regional expression differences between white and grey matter for HLA-I (K) and CCL2 (L) in FCD 2b lesions. HLA-I expression could be found in Olig2 and NeuN expressing cells ($K_{1,2}$). Comparison of vimentin$^+$ BCs (asterisks in M) to HLA-II expression revealed a strong correlation (M). Moreover, HLA-II expression was negatively correlated with Olig2 (N) and MBP expression (O). Sections B, C, F, G, J and K were counterstained with haematoxylin. Scale bars: 300 µm in B (representative for F,J), 50 µm in C (representative for G,K,L), 10 µm in K_1, 25 µm in K_2, 100 µm in O, arrows = DNs; asterisk = BCs. Mann–Whitney *U*-test and Spearman's rank test. Data are displayed as scatter plot (green = FCD 2b; blue = FCD 2a) with median (A,D,E,H) or slope (M,N); $^{**}p < 0.01$, $^{***}p < 0.001$. Asterisks in I indicate significant upregulation in FCD 2b. A,E $n = 6$ FCD 2a and $n = 10$ FCD 2b cases; D,H $n = 8$ FCD 2b cases, I $n = 11$ FCD 2a and $n = 20$ FCD 2b cases, J $n = 13$ FCD 2a and 19 FCD 2b cases, M, N $n = 4$ different images from 8 FCD 2b cases, O $n = 4$ different images from 7 FCD 2b cases. BC, balloon cell; DN, dysmorphic neuron; FCD, focal cortical dysplasia

DISCUSSION

Focal cortical dysplasia type 2 lesions are characterised by activation of innate and adaptive immune responses. Here, we show for the first time that FCD 2b lesions harbour an exaggerated intraparenchymal accumulation of peripheral immune cells, exaggerated antigen presentation and complement expression as compared to FCD 2a lesions. Moreover, these findings concentrate in the WM and correlate strongly with WM damage and BC number. These novel insights could aid in early stratification of patients and consequently more targeted therapy.

While FCD 2 is highly epileptogenic, the impact of BCs in FCD 2b in relation to epileptogenesis and co-morbidities remains limited. So far, most studies investigating activation of the immune system and neuroinflammation omitted to discriminate between 2a and 2b [18–23]. Direct comparison of differential expression between surgically resected tissue from FCD 2a and FCD 2b yielded only one differentially expressed gene after correction for multiple comparisons, melanophilin (*MLPH*; $p = 0.0055$). Although mutations in melanophilin are linked to changes in immune system function in patients with the rare autosomal Griscelli syndrome 3, its role in FCD warrants further investigation [30]. Differential expression of only one gene indicates that RNA expression in 2a and 2b is much more similar to each other than to age-matched controls. By comparing the datasets of FCD 2a versus control and FCD 2b versus control, we resolved more subtle differences in RNA expression which were confirmed via immunohistochemistry. We found specifically in FCD 2b T-lymphocyte infiltration as well as higher CD68, TSPO and HLA class II expression by monocytes and microglia, which correlated strongly with the number of BCs. This difference could not result from seizure activity, since seizure frequency in our cohort did not differ. Interestingly, BCs also expressed TSPO and HLA-II and were shown previously to express components of the IL-1β system [24], TLR-4 and COX-2 [31] making them highly immunogenic. The driving force behind the immunogenic expression profile could originate from the high mutational load and resulting intrinsic mTOR activation [9]. For instance, antigen presentation via HLA-II [32] and IL-1β expression [33] was shown to depend on the mTOR pathway. Moreover, the general anabolic activity mediated by mTOR hyperactivity [16] likely facilitates unspecific production of immune factors. To this end, in vitro manipulation of isolated BCs was shown before [34] and might pose a valuable resource to investigate functionality further.

We were interested whether other mechanisms of BC-dependent immune cell attraction or activation exist. Indeed, BCs displayed strong expression of CCL2 and CCL19 which could facilitate monocyte and T-lymphocyte homing to the brain parenchyma [35]. Dysfunction of the blood–brain barrier (BBB) and leukocyte infiltration are common during seizure activity and chronic epilepsy [36,37]. However, negligible T-lymphocyte infiltration could be detected in our FCD 2a cohort. Considering that seizure frequency between the FCD 2a and 2b cohorts was not different, this finding suggests that BCs or the immune response evoked by them are involved in peripheral immune cell invasion. Interestingly, albumin extravasation from blood vessels into the brain parenchyma was shown to be higher in FCD 2b, indicating that BBB dysfunction is more severe [23]. These findings are in agreement with a recent study showing that BC/GC containing FCD 2b/TSC lesions express a distinct inflammatory secretome profile from FCD 2a lesions without BCs [38]. Here, higher CCL2 expression was demonstrated in microglia in close proximity to BCs, suggesting complex intercellular interactions and an additional pro-inflammatory contribution from glial cells. While this study did not find CCL2 expression in BCs as the current study, higher CCL2 expression in microglia in organotypic cultures from FCD 2b lesions was sensitive to mTOR-pathway inhibition via everolimus. Thus, this finding supports a role for the mTOR pathway and BCs as driver of gene expression involved in immune cell attraction.

Recruitment of the peripheral immune system in FCD was shown before using flow cytometry of freshly resected tissue [19,20]. These studies concluded that peripherally derived, infiltrating myeloid and lymphoid immune cells play an important role in the inflammatory processes in FCD. Although we did not specifically discriminate resident from peripherally derived immune cells, we did not find differences in microglia density, but an increase in CD68 expression, which could originate from peripheral myeloid cells. Moreover, we detected intravascular lymphocytes in both pathologies. The fact that Xu et al. [20] did not detect a difference in lymphocyte number between FCD 2a and FCD 2b in their study indicates that intravascular lymphocyte migration to the brain is common in both pathologies, whereas we found that tissue infiltration seems to be specific to FCD 2b. Interestingly, both studies found evidence that some of the detected lymphocytes were antigen experienced, making them immunocompetent without requiring antigen presentation. This indicates that the infiltrating $CD8^+$ T lymphocytes in FCD 2b might be directly cytotoxic. Double labelling for oligodendrocytes and neurons confirmed expression of HLA-I in these cells, making interaction with $CD8^+$ T lymphocytes probable. These findings are corroborated by another study showing the apoptosis markers cleaved caspase-3 and terminal deoxynucleotidyl transferase dUTP nick end labelling (TUNEL) in FCD 2b lesions in several cell types such as DN and oligodendrocytes, but not $HLA\text{-}II^+$ leukocytes [39]. Moreover, these markers were stronger in FCD 2b compared to 2a and strongest in FCD 2b WM [39].

Comparison of the complement components from the differential expression analysis between FCD 2a and FCD 2b revealed a stronger activation of the complement system in FCD 2b lesions. This finding is supported by our previous study showing higher complement expression in FCD 2 [18]. In conjunction with the RNA-Seq data, we found extracellular accumulation of C1q in the neuropil surrounding BC-rich regions. Moreover, WM displayed very strong C1q reactivity in neuronal processes and sparse C1q reactivity was detected around vessels, implying BBB disruption. In contrast, C3d expression was found predominantly in and around dysmorphic cells and glia. The role of complement factors in the elimination of synapses during neurodevelopment [40], clearance of neurons and promotion of cytokine production [41] as well as its involvement in

epileptogenesis [42] suggests that the accumulation of C1q and C3d around BCs could greatly affect local connectivity and neuroinflammatory state. It is worth noting that we did not find reactivity for the membrane attack complex (C9neo), indicating that dysfunction is not mediated via the terminal step in the complement cascade.

Considering the strong similarities of the histopathology between FCD 2b and TSC, GCs in TSC were shown to appear before DN and displayed expression of inflammatory mediators already prenatally, before the occurrence of seizures [43]. Assuming similar mechanisms in FCD 2b lesions, early CCL2 and CCL19 expression by BCs could promote a continuous influx of immune cells into the developing brain. This very early, and stronger activation of the immune system in FCD 2b suggests a stronger role of immune system activation and inflammation during epileptogenesis. Consequently, the high epileptogenicity of FCD 2a might be rather based on the overall higher number of DN and resulting aberrant circuitry. Interestingly, the higher density of DN in FCD 2a compared to FCD 2b might be explained by the early infiltration of $CD8^+$ cytotoxic T lymphocytes. This is further supported by the strong expression of HLA-I in DN in both FCD subtypes, which has a higher probability to interact with intra-parenchymal T lymphocytes in FCD 2b.

Although our study shows significant tissue infiltration of peripherally derived immune cells and antigen presentation in FCD 2b, FCD 2a lesions still represent a pro-inflammatory environment as indicated by our RNA-Seq data. In addition, we found that DN express pro-inflammatory and ictogenic factors such as IL-17 and COX-2 [20,44,45]. Here, COX-2 expression was shown previously to be suppressed by mTORC1 and its activation in FCD 2 might result in COX-2 overexpression. The role of IL-17 in neuronal excitability and seizure susceptibility was shown before, but predominantly assigned to immune cells, not DN [20]. Additionally, it cannot be excluded that immune cell homing to the brain vasculature or immune factors entering the brain parenchyma are elevated in FCD 2a and exert their effect on resident immune cells. Moreover, microglia activation is evident in both pathologies [21].

Initially, we aimed to assess genotype effects on inflammation; however, due to statistical power, we focused on the comparison of FCD 2a versus FCD 2b. Nonetheless, genotype, variant allele frequency and timing of the mutation likely exert a strong influence on the presence or absence of BCs and consequently the extent of BC-mediated immune system activation we identified. Since the identified somatic mutations are not equally distributed across FCD 2a and 2b, we cannot explicitly exclude that the difference we identified stems primarily from mutations in the mTOR pathway. However, the single FCD 2a case with an *MTOR* mutation, as well as the FCD 2b case with *TSC1* mutation aligned with the other subtype-specific cases. This suggests that despite somatic mutations in *MTOR*, BCs and the surrounding tissue in FCD 2b display stronger immune system activation and neuroinflammation. Advances in sequencing technologies in terms of throughput and sensitivity will hopefully allow it to compare 2a versus 2b cases with the same genotype in the future.

Genotype discrimination might have therapeutic implications, since prenatal immune system activation in response to infection has been correlated with neurocognitive disabilities such as intellectual disability (ID) [46–48]. Hence, early anti-inflammatory treatment in FCD 2b could potentially benefit neurocognitive co-morbidities, which are frequently encountered in FCD [49–51]. Evidence from TSC suggests that aberrant WM development might be associated with autism spectrum disorder and ID [8,52]; thus, the cytotoxic microenvironment in the subcortical WM in FCD 2b lesions we identified suggests similar mechanisms. This is supported by previous studies linking mTOR activation in FCD 2b to myelin pathology [7,39].

Lastly, we identified that TSPO expression accurately reflects inflammation in FCD 2 lesions. TSPO can be targeted by positron emission tomography ligands and was previously utilised in the investigation of inflammation in epilepsy, including one FCD case study [53–55]. Consequently, TSPO might pose an attractive target for the diagnostic discrimination of inflammation and, potentially, FCD 2a and FCD 2b without invasive surgery.

In this study, we found stronger recruitment and activation of the immune system in FCD 2b lesions compared to FCD 2a. Our results indicate that BCs might be immunogenic during brain development and that targeting this aberrant process might improve WM integrity and associated co-morbidities in FCD 2b patients.

ACKNOWLEDGEMENTS

The research leading to these results has received funding from the European Union's Seventh Framework Programme (FP7/2007–2013) under grant agreement no. 602391 (EPISTOP; EA, FJ) and no. 602102 (EPITARGET; EAvV, EA), the European Union's Horizon 2020 WIDESPREAD-05-2020–Twinning (EpiEpiNet; EA, EAvV), grant agreement no. 952455, the Dutch Epilepsy Foundation, project number 16-05, 20-11 (DWMB, EAvV) and 20-02 (AM, ML); the European Union's Horizon 2020 Research and Innovation Programme under the Marie Sklodowska-Curie grant agreement no. 722053 (EU-GliaPhD; TSZ, EA); ZonMw, Programme Translational Research no. 95105004 (EA); an unrestricted grant from UCB Pharma (AE, JM); Prinses Beatrix Spierfonds, Grant application no: W.OR14 to Frank Baas (IM).

CONFLICT OF INTEREST

LF, JVE and SD were employees of UCB Pharma at the time of research. AE and JM are financially supported by an unrestricted grant from UCB Pharma.

AUTHOR CONTRIBUTION

TSZ, DWMB, ML, CM, JJA, IM, LF, JvE and JDM performed the experiments, data collection and analysis. FEJ, PCvR, NSS, JHL, SD, AM and EA helped with the selection and collection of human brain tissues and clinical data. EA and JDM conceived the study and participated in its design and coordination. TSZ, SD, EAvV, AM, JDM and EA drafted and prepared the manuscript. All authors read, revised and approved the final manuscript.

ETHICAL APPROVAL

All procedures performed in studies involving human participants were in accordance with the Amsterdam UMC Research Code provided by the Medical Ethics Committee and with the 1964 Helsinki declaration and its later amendments or comparable ethical standards.

PEER REVIEW

The peer review history for this article is available at https://publons.com/publon/10.1111/nan.12736.

DATA AVAILABILITY STATEMENT

The data that support the findings of this study are available from UCB Pharma. Restrictions apply to the availability of these data, which were used under license for this study. Data are available via the corresponding author with the permission of UCB Pharma.

ORCID

Till S. Zimmer https://orcid.org/0000-0002-6869-3697
Diede W. M. Broekaart https://orcid.org/0000-0002-4842-0659
Erwin A. van Vliet https://orcid.org/0000-0001-5747-3202
Angelika Mühlebner https://orcid.org/0000-0001-9102-7353
Eleonora Aronica https://orcid.org/0000-0002-3542-3770

REFERENCES

1. Blumcke I, Spreafico R, Haaker G, et al. Histopathological findings in brain tissue obtained during epilepsy surgery. *N Engl J Med*. 2017;377(17):1648-1656.
2. Blumcke I, Thom M, Aronica E, et al. The clinicopathologic spectrum of focal cortical dysplasias: a consensus classification proposed by an ad hoc Task Force of the ILAE Diagnostic Methods Commission. *Epilepsia*. 2011;52(1):158-174.
3. Najm IM, Sarnat HB, Blumcke I. Review: The international consensus classification of Focal Cortical Dysplasia—a critical update 2018. *Neuropathol Appl Neurobiol*. 2018;44(1):18-31.
4. Mizuguchi M, Takashima S. Neuropathology of tuberous sclerosis. *Brain Dev*. 2001;23(7):508-515.
5. Colombo N, Tassi L, Deleo F, et al. Focal cortical dysplasia type IIa and IIb: MRI aspects in 118 cases proven by histopathology. *Neuroradiology*. 2012;54(10):1065-1077.
6. Muhlebner A, Coras R, Kobow K, et al. Neuropathologic measurements in focal cortical dysplasias: validation of the ILAE 2011 classification system and diagnostic implications for MRI. *Acta Neuropathol*. 2012;123(2):259-272.
7. Scholl T, Muhlebner A, Ricken G, et al. Impaired oligodendroglial turnover is associated with myelin pathology in focal cortical dysplasia and tuberous sclerosis complex. *Brain Pathol*. 2017;27(6):770-780.
8. Muhlebner A, van Scheppingen J, de Neef A, et al. Myelin pathology beyond white matter in tuberous sclerosis complex (TSC) cortical tubers. *J Neuropathol Exp Neurol*. 2020;79(10):1054-1064.
9. Baldassari S, Ribierre T, Marsan E, et al. Dissecting the genetic basis of focal cortical dysplasia: a large cohort study. *Acta Neuropathol*. 2019;138(6):885-900.
10. Baulac S, Ishida S, Marsan E, et al. Familial focal epilepsy with focal cortical dysplasia due to DEPDC5 mutations. *Ann Neurol*. 2015;77(4):675-683.
11. D'Gama AM, Woodworth MB, Hossain AA, et al. Somatic mutations activating the mTOR pathway in dorsal telencephalic progenitors cause a continuum of cortical dysplasias. *Cell Rep*. 2017;21(13):3754-3766.
12. Lim JS, Gopalappa R, Kim SH, et al. Somatic mutations in TSC1 and TSC2 cause focal cortical dysplasia. *Am J Hum Genet*. 2017;100(3):454-472.
13. Lim JS, Kim WI, Kang HC, et al. Brain somatic mutations in MTOR cause focal cortical dysplasia type II leading to intractable epilepsy. *Nat Med*. 2015;21(4):395-400.
14. Sim JC, Scerri T, Fanjul-Fernandez M, et al. Familial cortical dysplasia caused by mutation in the mammalian target of rapamycin regulator NPRL3. *Ann Neurol*. 2016;79(1):132-137.
15. Sim NS, Ko A, Kim WK, et al. Precise detection of low-level somatic mutation in resected epilepsy brain tissue. *Acta Neuropathol*. 2019;138(6):901-912.
16. Saxton RA, Sabatini DM. mTOR signaling in growth, metabolism, and disease. *Cell*. 2017;168(6):960-976.
17. Aronica E, Crino PB. Inflammation in epilepsy: clinical observations. *Epilepsia*. 2011;52(Suppl 3):26-32.
18. Iyer A, Zurolo E, Spliet WG, et al. Evaluation of the innate and adaptive immunity in type I and type II focal cortical dysplasias. *Epilepsia*. 2010;51(9):1763-1773.
19. Owens GC, Garcia AJ, Mochizuki AY, et al. Evidence for innate and adaptive immune responses in a cohort of intractable pediatric epilepsy surgery patients. *Front Immunol*. 2019;10:121.
20. Xu D, Robinson AP, Ishii T, et al. Peripherally derived T regulatory and gammadelta T cells have opposing roles in the pathogenesis of intractable pediatric epilepsy. *J Exp Med*. 2018;215(4):1169-1186.
21. Boer K, Spliet WG, van Rijen PC, Redeker S, Troost D, Aronica E. Evidence of activated microglia in focal cortical dysplasia. *J Neuroimmunol*. 2006;173(1–2):188-195.
22. Zhang Z, Liu Q, Liu M, et al. Upregulation of HMGB1-TLR4 inflammatory pathway in focal cortical dysplasia type II. *J Neuroinflammation*. 2018;15(1):27.
23. Prabowo AS, Iyer AM, Anink JJ, Spliet WG, van Rijen PC, Aronica E. Differential expression of major histocompatibility complex class I in developmental glioneuronal lesions. *J Neuroinflammation*. 2013;10:12.
24. Ravizza T, Boer K, Redeker S, et al. The IL-1beta system in epilepsy-associated malformations of cortical development. *Neurobiol Dis*. 2006;24(1):128-143.
25. Vezzani A, Lang B, Aronica E. Immunity and inflammation in epilepsy. *Cold Spring Harb Perspect Med*. 2015;6(2):a022699.
26. Vezzani A, Balosso S, Ravizza T. Neuroinflammatory pathways as treatment targets and biomarkers in epilepsy. *Nat Rev Neurol*. 2019;15(8):459-472.
27. Croft D, Mundo AF, Haw R, et al. The Reactome pathway knowledgebase. *Nucleic Acids Res*. 2014;42(D1):D472-D477.
28. Huang DW, Sherman BT, Tan Q, et al. DAVID Bioinformatics resources: expanded annotation database and novel algorithms to better extract biology from large gene lists. *Nucleic Acids Res*. 2007;35(Suppl 2):W169-W175.
29. Kohl M, Wiese S, Warscheid B. Cytoscape: software for visualization and analysis of biological networks. *Methods Mol Biol*. 2011;696:291-303.
30. Menasche G, Ho CH, Sanal O, et al. Griscelli syndrome restricted to hypopigmentation results from a melanophilin defect (GS3) or a MYO5A F-exon deletion (GS1). *J Clin Invest*. 2003;112(3):450-456.
31. Arena A, Zimmer TS, van Scheppingen J, et al. Oxidative stress and inflammation in a spectrum of epileptogenic cortical malformations: molecular insights into their interdependence. *Brain Pathol*. 2019;29(3):351-365.
32. Saric A, Hipolito VE, Kay JG, Canton J, Antonescu CN, Botelho RJ. mTOR controls lysosome tubulation and antigen presentation in macrophages and dendritic cells. *Mol Biol Cell*. 2016;27(2):321-333.
33. Yang T, Zhu L, Zhai Y, et al. TSC1 controls IL-1beta expression in macrophages via mTORC1-dependent C/EBPbeta pathway. *Cell Mol Immunol*. 2016;13(5):640-650.

34. Yasin SA, Latak K, Becherini F, et al. Balloon cells in human cortical dysplasia and tuberous sclerosis: isolation of a pathological progenitor-like cell. *Acta Neuropathol*. 2010;120(1):85-96.
35. Sokol CL, Luster AD. The chemokine system in innate immunity. *Cold Spring Harb Perspect Biol*. 2015;7(5):a016303.
36. Gorter JA, van Vliet EA, Aronica E. Status epilepticus, blood-brain barrier disruption, inflammation, and epileptogenesis. *Epilepsy Behav*. 2015;49:13-16.
37. van Vliet EA, Aronica E, Gorter JA. Role of blood-brain barrier in temporal lobe epilepsy and pharmacoresistance. *Neuroscience*. 2014;277:455-473.
38. Li YF, Scerif F, Picker SR, et al. Identifying cellular signalling molecules in developmental disorders of the brain: Evidence from focal cortical dysplasia and tuberous sclerosis. *Neuropathol Appl Neurobiol*. 2021. https://doi.org/10.1111/nan.12715.
39. Iyer A, Prabowo A, Anink J, Spliet WG, van Rijen PC, Aronica E. Cell injury and premature neurodegeneration in focal malformations of cortical development. *Brain Pathol*. 2014;24(1):1-17.
40. Stevens B, Allen NJ, Vazquez LE, et al. The classical complement cascade mediates CNS synapse elimination. *Cell*. 2007;131(6):1164-1178.
41. Fraser DA, Pisalyaput K, Tenner AJ. C1q enhances microglial clearance of apoptotic neurons and neuronal blebs, and modulates subsequent inflammatory cytokine production. *J Neurochem*. 2010;112(3):733-743.
42. Chu Y, Jin X, Parada I, et al. Enhanced synaptic connectivity and epilepsy in C1q knockout mice. *Proc Natl Acad Sci U S A*. 2010;107(17):7975-7980.
43. Prabowo AS, Anink JJ, Lammens M, et al. Fetal brain lesions in tuberous sclerosis complex: TORC1 activation and inflammation. *Brain Pathol*. 2013;23(1):45-59.
44. Rojas A, Jiang J, Ganesh T, et al. Cyclooxygenase-2 in epilepsy. *Epilepsia*. 2014;55(1):17-25.
45. Aronica E, Bauer S, Bozzi Y, et al. Neuroinflammatory targets and treatments for epilepsy validated in experimental models. *Epilepsia*. 2017;58(Suppl 3):27-38.
46. Hughes HK, Mills Ko E, Rose D, Ashwood P. Immune dysfunction and autoimmunity as pathological mechanisms in autism spectrum disorders. *Front Cell Neurosci*. 2018;12:405.
47. Jones KL, Croen LA, Yoshida CK, et al. Autism with intellectual disability is associated with increased levels of maternal cytokines and chemokines during gestation. *Mol Psychiatry*. 2017;22(2):273-279.
48. Meltzer A, Van de Water J. The role of the immune system in autism spectrum disorder. *Neuropsychopharmacology*. 2017;42(1):284-298.
49. Braun KP. Preventing cognitive impairment in children with epilepsy. *Curr Opin Neurol*. 2017;30(2):140-147.
50. Kimura N, Takahashi Y, Shigematsu H, et al. Risk factors of cognitive impairment in pediatric epilepsy patients with focal cortical dysplasia. *Brain Dev*. 2019;41(1):77-84.
51. Kwon HE, Eom S, Kang HC, et al. Surgical treatment of pediatric focal cortical dysplasia: clinical spectrum and surgical outcome. *Neurology*. 2016;87(9):945-951.
52. Prohl AK, Scherrer B, Tomas-Fernandez X, et al. Early white matter development is abnormal in tuberous sclerosis complex patients who develop autism spectrum disorder. *J Neurodev Disord*. 2019;11(1):36.
53. Dickstein LP, Liow JS, Austermuehle A, et al. Neuroinflammation in neocortical epilepsy measured by PET imaging of translocator protein. *Epilepsia*. 2019;60(6):1248-1254.
54. Gershen LD, Zanotti-Fregonara P, Dustin IH, et al. Neuroinflammation in temporal lobe epilepsy measured using positron emission tomographic imaging of translocator protein. *JAMA Neurol*. 2015;72(8):882-888.
55. Butler T, Ichise M, Teich AF, et al. Imaging inflammation in a patient with epilepsy due to focal cortical dysplasia. *J Neuroimaging*. 2013;23(1):129-131.

SUPPORTING INFORMATION

Additional supporting information may be found online in the Supporting Information section.

How to cite this article: Zimmer TS, Broekaart DWM, Luinenburg M, et al. Balloon cells promote immune system activation in focal cortical dysplasia type 2b. *Neuropathol Appl Neurobiol*. 2021;47:826–839. https://doi.org/10.1111/nan.12736